Monitoring avalanche activity using a seismic sensor

A. van Herwijnen [a,b,*], J. Schweizer [a]

[a] *WSL Institute for Snow and Avalanche Research SLF, Davos, Switzerland*
[b] *Montana Sate University, Department of Civil Engineering, Bozeman, Montana, USA*

ARTICLE INFO

ABSTRACT

Avalanche activity data represent the most direct instability data for avalanche forecasting. Yet, avalanche observations are notoriously incomplete. With remote avalanche detection methods this deficiency might be overcome. We used a geophone buried in the snowpack to monitor avalanche activity. Contrary to previous studies we inserted the geophone directly in an avalanche start zone, allowing for the detection of substantially smaller avalanches, including loose snow avalanches. The observed patterns in the signals generated by different types of avalanches qualitatively confirmed previous work. By visually analyzing the spectrogram of the seismic data, over 380 avalanches were identified during the winter of 2010 over an area of about 2 km^2. Avalanche activity was also monitored with two automatic cameras. Avalanche activity data obtained from the seismic sensor and from automatic cameras were in good agreement. Our field observations suggest that slab avalanches were better detected than loose snow avalanches. The relation between avalanche activity and meteorological data were in line with commonly followed rules in avalanche forecasting. Our results confirm that avalanche detection using seismic methods can provide reliable avalanche activity data for avalanche forecasting.

© 2011 Elsevier B.V. All rights reserved.

1. Introduction

Data on avalanche activity are of paramount importance for avalanche forecasting (McClung and Schaerer, 2006). Avalanche activity is usually estimated based on visual observations, which are imprecise and impossible at night or when visibility is limited. This often leads to uncertainties in the number and exact timing of avalanches, resulting in a poor correlation between avalanche activity and estimated avalanche danger (e.g. Schweizer et al., 2003). To obtain more objective avalanche activity data, two different types of automatic avalanche detection systems have been developed. First, with infra-sound monitoring, low frequency sound waves (below 20 Hz) generated by avalanches are detected using microphones (e.g. Scott et al., 2007). Second, with seismic avalanche detection ground motion generated by the down-slope movement of avalanches is recorded using geophones (e.g. Navarre et al., 2009).

Seismic sensors are very well suited for the remote detection of hazardous mass movements such as rockfall, landslides and snow avalanches (e.g. Deparis et al., 2008; Suriñach et al., 2005). St.Lawrence and Williams (1976) were the first to show that seismic methods can be used to detect avalanches. Studies on seismic signals generated by avalanches have essentially two main goals: improving our understanding of avalanche dynamics and monitoring avalanche activity.

Seismic methods have been used to determine characteristics of snow avalanches. The recorded seismic time series are complex since they are generated by multiple moving sources interacting with local topography in combination with complex wave propagation in heterogeneous media (Suriñach et al., 2005). Nevertheless, basic seismic signatures for snow avalanches, i.e. a 'spindle' shape in the seismograms (i.e. seismic time series) and a triangular shape in the spectrograms (i.e. time-frequency plot), are well documented (e.g. Biescas et al., 2003; Nishimura and Izumi, 1997; Suriñach et al., 2000). Detailed analysis of seismic signals generated by avalanches in conjuncture with video records revealed that increases in signal amplitude coincided with impacts of the flowing snow mass with terrain features and obstacles (Sabot et al., 1998; Suriñach et al., 2000, 2001). Biescas et al. (2003) compared avalanches of similar runout distance and showed that wet snow avalanches generate signals that are larger than those generated by dry snow avalanches, likely due to the higher density of the mass involved. More recently, the speed of avalanches (Vilajosana et al., 2007a) as well as the energy transmitted into the ground (Vilajosana et al., 2007b) were estimated from seismic observations. These studies provide increasingly valuable information on snow avalanche dynamics and highlight the importance of the location of the sensor relative to the avalanche, local site effects, geometrical spreading with distance and dispersive anelastic energy attenuation. However, in order to analyze the seismic signals in great detail sophisticated equipment in a single avalanche path is required and only a few avalanches can be investigated.

Automatic avalanche monitoring systems, on the other hand, employ seismic sensors to derive information about avalanche activity.

* Corresponding author at: WSL Institute for Snow and Avalanche Research SLF, Davos, Switzerland.
E-mail address: afg_herwijn@yahoo.ca (A. van Herwijnen).

These systems typically rely on a few seismic sensors in an avalanche track or at valley bottom to detect avalanches (e.g. Bessason et al., 2007; Navarre et al., 2009). Avalanches that occur up to several kilometers away from the sensors can be detected, depending on the size of the event (e.g. Leprettre et al., 1998). Automatic avalanche detection is based on event detection using an amplitude threshold and event classification. Signal interpretation is relatively limited and due to the amplitude threshold only larger avalanches are registered. While there has been progress in signal classification, positive identification of avalanches remains problematic (Bessason et al., 2007; Navarre et al., 2009). Therefore, thus far automatic avalanche monitoring systems are not widely used.

We have developed a seismic sensor array to continuously monitor an avalanche start zone with the goal to capture precursor signals to avalanche release (van Herwijnen and Schweizer, 2011). So far, precursor signals to avalanche release have not been identified. However, avalanches were very well detected. In combination with images from two automatic cameras we were able to identify numerous seismic signals generated by avalanches. Here we present qualitative characteristics of signals generated by avalanches, confirming findings from previous studies. Furthermore, we use a simple visual approach to derive avalanche activity data from the seismic data for the entire winter of 2010. Finally, we relate avalanche activity to meteorological data from nearby automatic meteorological stations (AMS). The main goal is to evaluate the reliability and limitations of avalanche detection using seismic methods.

2. Field site and instrumentation

The seismic data which were analyzed came from a geophone which was part of a sensor array deployed on an avalanche start zone in the Eastern Swiss Alps near Davos, Switzerland. The field site and the sensor array are briefly described; a detailed description can be found in van Herwijnen and Schweizer (2011). The sensor array was deployed in a field site located approximately 2.5 km above the town of Davos. Three ski areas are within a five kilometer radius of the site (Fig. 1). The field site is instrumented with seven AMSs providing continuous meteorological data. One AMS is within 50 m of the sensor array and two additional AMSs are within 200 m of the sensor array (Fig. 1).

The sensor array was deployed on a steep NE facing avalanche start zone at 2475 m.a.s.l. on the lee side of a ridge (Fig. 2). It consisted of six geophones inserted in the snow cover and one geophone inserted in the ground. The sensor in the ground was installed early in the season before the first snowfall. To improve the coupling between the other sensors and the snow, the remaining six geophones were
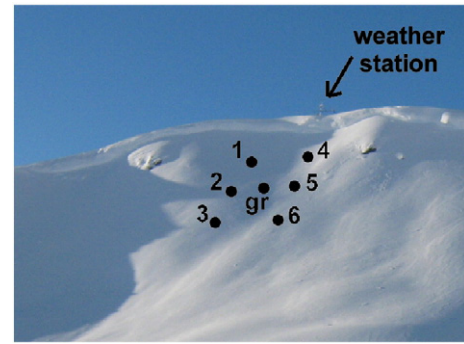

Fig. 2. Deployment configuration of the geophone array. Six geophones (1 to 6) were installed in a rectangular configuration with a 5 m sensor spacing. One geophone was inserted in the ground (gr) in the middle of the rectangle. There is an automatic weather station at the top of the ridge within 50 m of the sensors.

mounted in a foam housing with a density close to that of snow (van Herwijnen and Schweizer, 2011). When the slope was covered by at least one meter of snow, the six sensors in the foam housing were placed on top of the snow cover to be buried by subsequent snowfall. These sensors were therefore approximately one meter above the ground, while the amount of snow above the sensors gradually increased during the entire winter. The sensors in the snow cover were placed in a rectangular configuration with a 5 m sensor spacing, while the sensor in the ground was in the middle (Fig. 2).

We used vertical uni-axial geophones with a natural frequency of 14 Hz (SM-6 14 Hz geophone; www.iongeo.com). The geophone is most sensitive at its natural frequency (about 80 V/ms^{-1}). Below 14 Hz the sensitivity rapidly decreases with a cutoff at 1 Hz, while the sensitivity is constant from about 40 to 1000 Hz (28.8 V/ms^{-1}). A low power 24-bit data acquisition system was used (Seismic Instruments SmartGeophone system). Data were continuously recorded at a sampling rate of 500 Hz and stored locally on a low power computer with a 30 day storage capacity. Approximately every 10 days the data were manually retrieved. We used a relatively high sampling rate because the sensor array was designed to investigate the existence of precursor signals to avalanche release, which are expected to consist of higher frequency signals (van Herwijnen and Schweizer, 2011).

Additional observation means, consisting of a microphone and two autonomous digital cameras, were installed to aid in the identification of sources of environmental noise (van Herwijnen and Schweizer, 2011). A standard desktop microphone with a response bandwidth between 0.1 and 16 kHz was mounted on the AMS at the top of the ridge. Acoustic data were continuously recorded at a sampling rate of
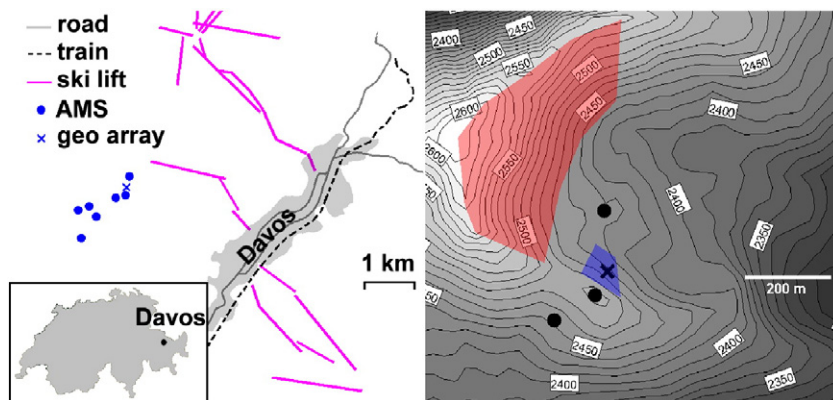

Fig. 1. Overview of the field site where the sensor array was deployed. Left: large scale view of the location of the sensor array (cross), automatic meteorological stations (AMS; dots), major roads (gray solid line), railways (black dashed line), ski lifts (pink solid lines) and the town of Davos (gray area). Right: close-up view of the location of the sensor array (cross) and the three nearest weather stations. Digital Elevation Model (DEM) from Federal Office of Topography (Swisstopo, http://www.swisstopo.ch/en/). The field of view of both the automatic cameras is indicated by the red and blue shaded areas.

4 kHz and stored locally with a 6 day storage capacity. Since the microphone was of low quality, it could only be used to identify sources of environmental noise. Acoustic signals generated by avalanches could not be identified. Two automatic 7 Mpixel digital cameras were mounted on the AMSs closest to the sensor slope. Camera 1 was directed at the sensor slope and camera 2 at a large NE to SE facing avalanche start zone to the west of the sensor slope (Fig. 1). Images were stored locally every 5 min. As for the seismic sensors, data from the microphone and the cameras were manually retrieved approximately every 10 days.

3. Data

During the winter of 2009–2010 continuous seismic data from the sensor array were collected from 12 January until the end of April (109 days). Data from one geophone inserted in the snow cover are analyzed in this study (sensor 1 in Fig. 2). We focus on the characteristics of signals generated by avalanches and avalanche activity for this sensor. However, all signals associated with avalanches recorded by sensor 1 were also recorded by the other geophones in the sensor array. A thorough comparison of data from the seven seismic sensors will be addressed in future work.

Due to the limited storage capacity for the microphone, there were 61 days of continuous acoustic data. The automatic cameras, had ample storage capacity. Camera 1 recorded images for the entire winter (109 days), while camera 2 was only installed on 1 February 2010 (89 days).

In order to compare avalanche activity to local meteorological conditions, data from the automatic meteorological stations in the immediate vicinity of the sensor array were used. We focussed on air temperature (Ta), wind speed (v) and snow height (HS), which were recorded at ten minute intervals.

4. Environmental noise

Proper characterization of signals generated by environmental noise was of paramount importance. Given the proximity of our field site to the town of Davos, as well as several ski areas (Fig. 1), there was considerable environmental noise in the seismic data. The automatic cameras as well as the microphone were instrumental in distinguishing seismic signals generated by avalanche from environmental noise. For our field site, van Herwijnen and Schweizer (2011) identified characteristics of seismic signals generated by the major sources of background noise: people walking, airplanes, explosives, earthquakes, helicopters, wind, snowcats and ski lifts. As an example, in Fig. 3 harmonic frequencies in

the acoustic and seismic data generated by a propeller airplane are clearly visible. Both the engine and propeller produce sounds which are periodic, since they originate in mechanical rotation mechanisms, resulting in clear harmonics (Buckingham et al., 2002). Furthermore, a Doppler effect is observed. Similar harmonic bands have been identified for helicopters in various studies investigating seismic signals and avalanche activity (e.g. Biescas et al., 2003; Navarre et al., 2009).

Past research has shown that seismic signals generated by avalanches have a unique frequency content evolution in time (e.g. Biescas et al., 2003; Suriñach et al., 2000). van Herwijnen and Schweizer (2011) showed that for our field site the spectrogram of signals generated by avalanches is different from that of most environmental noise. For the analysis presented here, spectrograms were calculated by the short time Fourier transform with a 500 samples length window with 50% overlap. Therefore, the signal was decomposed in 1 s time windows and 1 Hz frequency windows.

Using the spectrogram one can discriminate seismic signals generated by avalanches from environmental noise, as illustrated in Fig. 4. Note the constant band in the spectrogram around 14 Hz, here and in other figures, which stems from the increased sensitivity of the sensor at its natural frequency. In this example, the energy of the seismic signal generated by the avalanche was below 50 Hz (bottom Fig. 4). It is well known that the frequency content in the spectrogram of an avalanche depends on the distance between the avalanche and the sensor (e.g. Suriñach et al., 2005). However, as will be shown below, for the avalanches we observed the most energetic signals were generally below 50 Hz. On the other hand, most of the energy of signals generated by environmental noise was above 50 Hz (bottom Fig. 4). One exception are seismic signals generated by earthquakes, as also noted by Biescas et al. (2003) and Suriñach et al. (2005). Shown in Fig. 5 is the seismic signal generated by an earthquake of magnitude 1.6 located 22.8 km away from the sensor (Swiss Seismological Service). For the earthquake, most of the energy was also below the natural frequency of the geophone (i.e. below 14 Hz) while this was not the case for the avalanche where most of the energy was between 15 and 50 Hz (bottom Fig. 4).

5. Avalanche-generated signals

Based on field observations and the images from the automatic cameras we were able to identify numerous seismic signals generated by avalanches. We observed avalanches with a runout distance ranging from only a few meters to a maximum of approximately 350 meters. We determined that avalanches within at least an 850 m radius of the sensor array were detected, corresponding to an area of about 2 km^2. Here, we
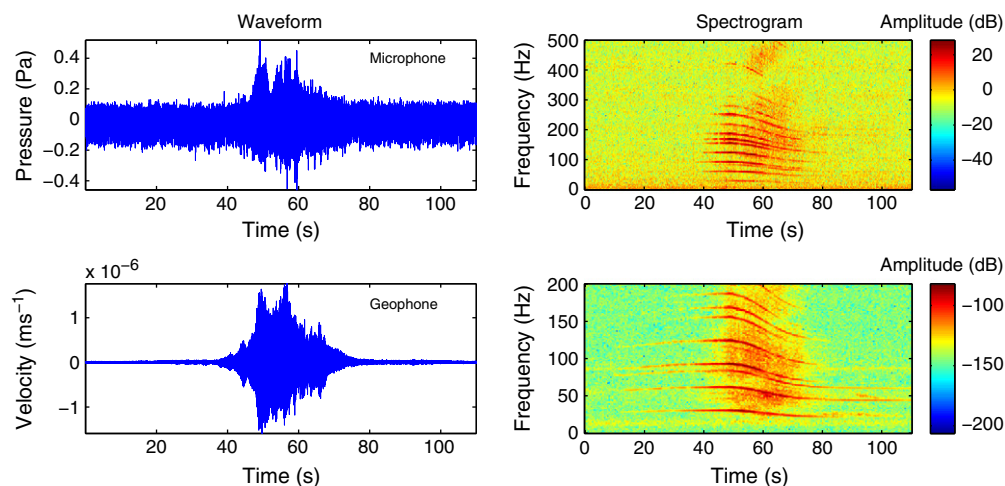

Fig. 3. Signal generated by a propeller airplane. Left: waveform. Right: spectrogram. Top: acoustic data recorded by the microphone. Bottom: seismic data recorded by the geophone. Harmonic frequencies, typical for propeller airplanes and helicopters, are clearly seen in the spectrogram.
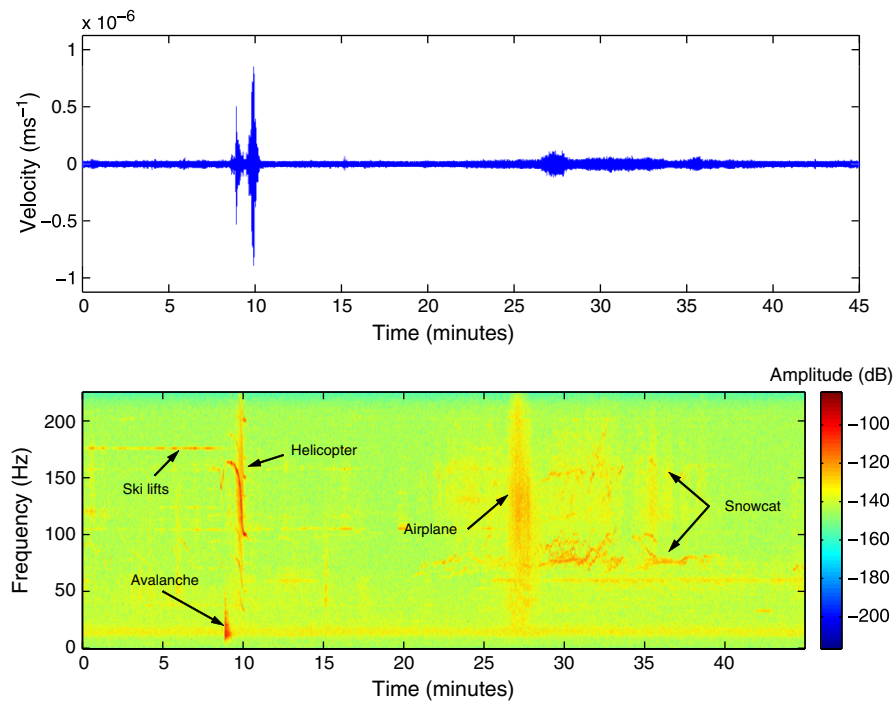
Fig. 4. Seismic signals generated by environmental noise as well as by a snow avalanche. Top: seismogram of 45 min of seismic data. Bottom: corresponding spectrogram. The spectral content of signals generated by environmental noise (i.e. ski lift, helicopter, airplane and snowcat) is different from that of a snow avalanche.

investigate typical characteristics of seismic signals generated by snow avalanches within our field site.

5.1. Loose snow avalanches

Loose snow avalanches originate at a single point on the snow surface gradually entraining more mass as the snow moves downslope.

Loose snow avalanches generate seismic signals which increase in amplitude as the mass of the avalanche increases (St.Lawrence and Williams, 1976; van Herwijnen and Schweizer, 2011). This is explained by the fact that as additional material is entrained into the moving mass, more energy is transmitted into the ground (Suriñach et al., 2005). During the winter of 2010, 157 loose snow avalanches were observed on the images of the automatic cameras. These consisted of both dry and
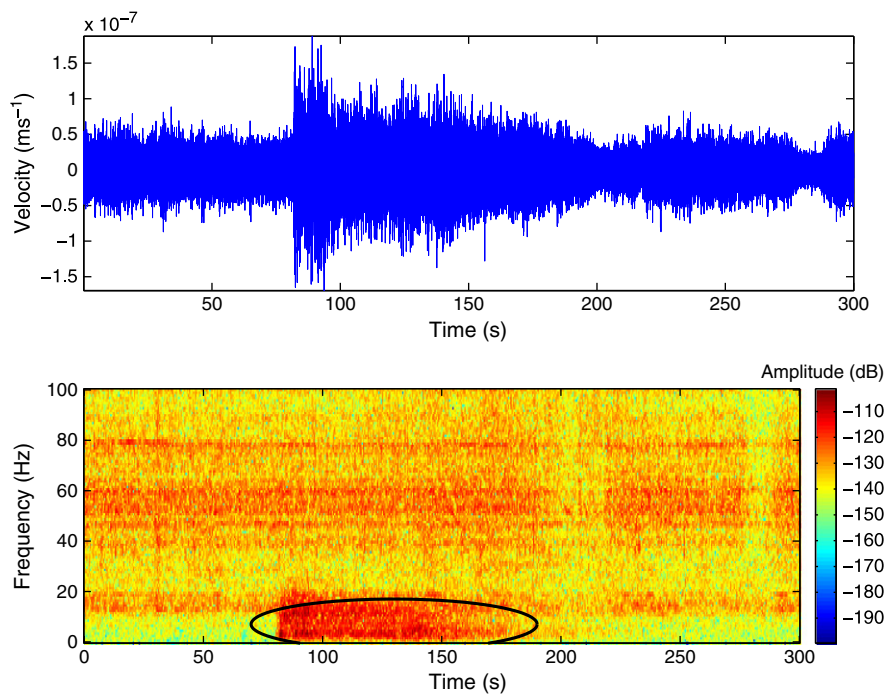

Fig. 5. Signal generated by an earthquake of magnitude 1.6 located 22.8 km away from the sensor (Swiss Seismological Service). Top: seismogram. Bottom: spectrogram. Most of the energy of the seismic signal generated by this earthquake was below 20 Hz (black ellipse). The energy between 40 and 60 Hz is attributed to noise from wind, while ski lifts generated the constant band at 80 Hz.

wet loose snow avalanches of a wide range of sizes. Here we discuss several loose snow avalanches which generated seismic signals recorded by the geophone as well as loose snow avalanches which were not recorded by the geophone.

The locations of seven loose snow avalanches that were linked to seismic signals recorded by the geophone are shown in Fig. 6. Avalanche 1 to 4 and avalanche 6 were wet loose snow avalanches which entrained the entire snow cover, while avalanche 5 and 7 were both surface loose snow avalanches consisting of dry and wet snow, respectively. Broadly speaking, the seismogram generated by these seven loose snow avalanches exhibited a typical spindle shape (Fig. 7). Sharp increases in the seismogram are attributed to the impact of the flowing snow mass with terrain features and are related to the local topography and ground cover (Biescas et al., 2003; Nishimura and Izumi, 1997; Suriñach et al., 2000; Vilajosana et al., 2007b). For instance, maxima in the seismogram for avalanche 1 to 4 and avalanche 6 were observed at the end of the events when the

avalanches abruptly came to a halt on more gentle terrain, commonly referred to as the stopping phase (e.g. Sabot et al., 1998).

Apart from local site effects, the amplitude and spectral content of seismic signals generated by avalanches relate more to the distance between the sensor and the avalanche than to the size of the avalanche (Suriñach et al., 2001). We observed similar trends with loose snow avalanches. Avalanche 7 was a very small loose snow avalanche which released close to the geophone (Fig. 6). The amplitude of the signal generated by this avalanche was larger than for most other loose snow avalanches shown in Fig. 7. Furthermore, while the majority of the energy of seismic signals generated by loose snow avalanches was below 40 Hz, this was not the case for avalanche 7 (Fig. 7). This comes as no surprise since the anelastic attenuation with distance of seismic waves is frequency dependent, i.e. high frequency signals attenuate much more rapidly than low frequency signals (Lay and Wallace, 1995). The amplitude of the seismic signals generated by loose snow avalanches is also related to the type of avalanche (i.e. wet or dry snow).
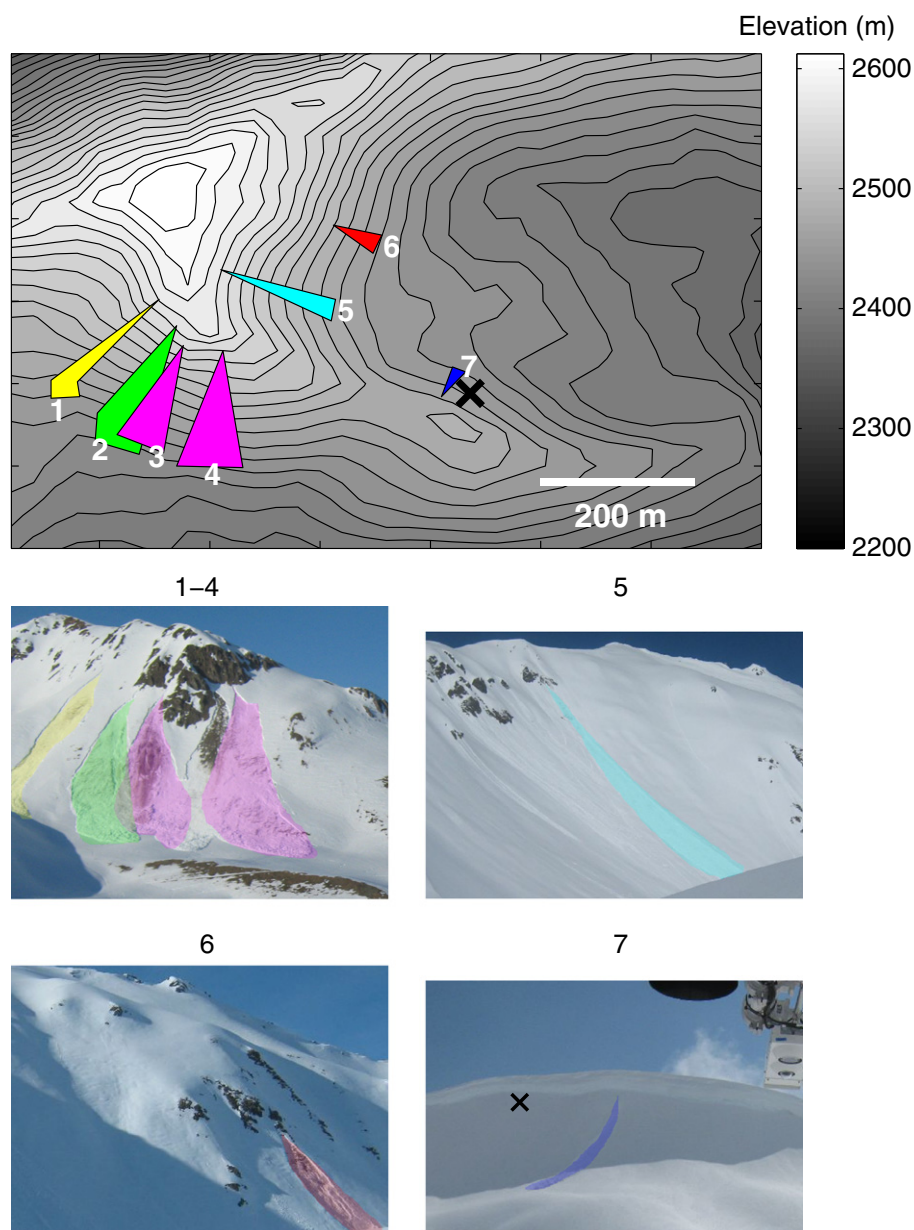

Fig. 6. Location of seven loose snow avalanches observed on the images from automatic cameras and detected in the seismic data. Top: approximate location and runout distance for each avalanche. The location of the geophone is marked with a black cross. Bottom: images from automatic cameras with the contour for each avalanche. The location of the geophone is marked with a black cross in the bottom right image.
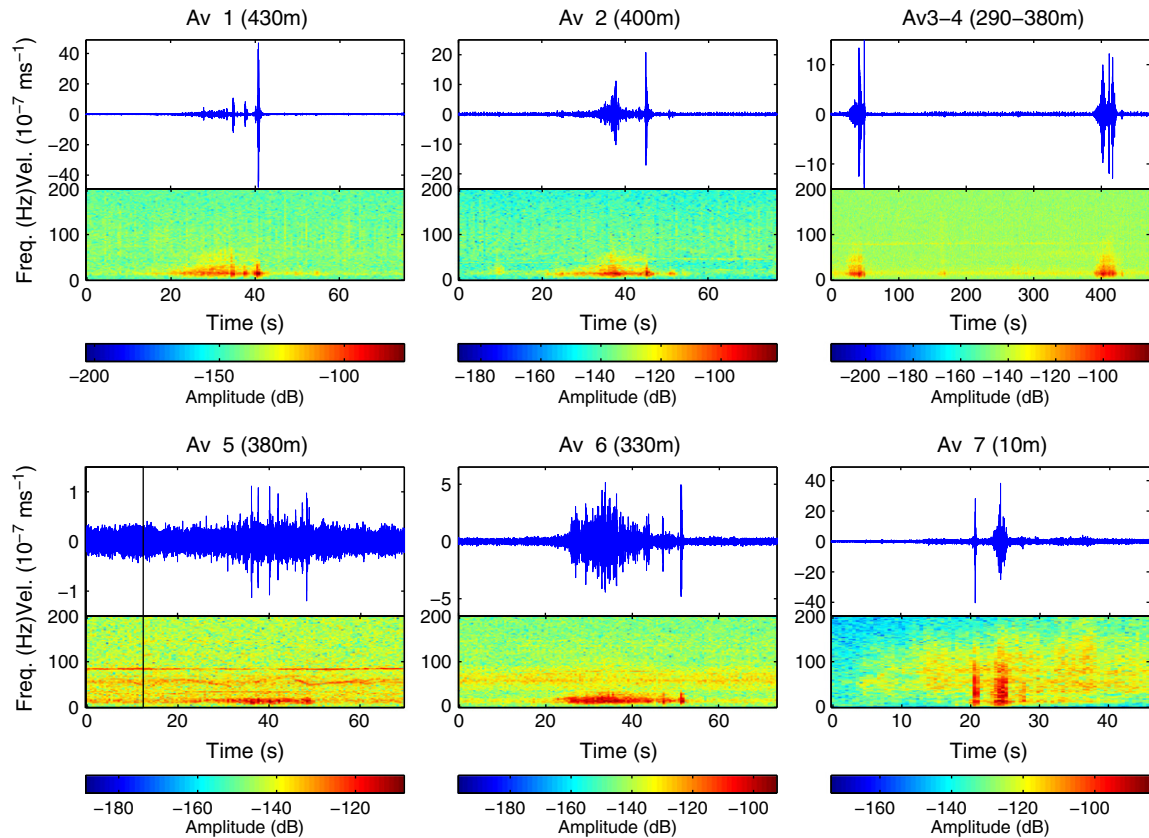
Fig. 7. Seismic signals generated by the seven loose snow avalanches shown in Fig. 6. For each avalanche the seismogram (top) and spectrogram (bottom) are shown. The approximate distance to the geophone is also given (in brackets). The seismic signals generated by avalanche 3 and 4 are shown together since these events appeared simultaneously on the images.

Avalanche 5 and 6, which were comparable in size and distance to the sensor (Fig. 6), exhibited very different signal amplitudes. The dry loose snow avalanche (avalanche 5) generated signals with much smaller amplitudes than the wet loose snow avalanche (avalanche 6).

Due to the attenuation of seismic waves with distance there is a limit to the size of avalanches that can be detected (Biescas et al., 2003; Suriñach et al., 2001). The geophone did not record the seismic signals generated by eight small dry loose snow avalanches which were observed on 21 February 2010 between 11:00 and 11:30 (Fig. 8). On the other hand, the seismic signals generated by nine wet loose snow avalanches which were observed in the same location on 23 March 2010 between 12:00 and 14:00 were recorded by the geophone (Fig. 9). These examples show that the type of snow involved in the avalanche is of importance as well, as suggested by (Biescas et al., 2003), albeit for much larger avalanches.

5.2. Snow slab avalanches

During the winter of 2010, 11 snow slab avalanches were observed on the images of the automatic cameras. All these avalanches were linked to seismic signals recorded by the geophone. Furthermore, the seismic signals of 9 additional slab avalanches, which were observed by field workers, were also found in the seismic signals recorded by the geophone. These mainly consisted of dry snow slab avalanches with a wide range of sizes. Here we discuss the seismic signals of 10 slab avalanches.

The locations of these ten slab avalanches which released within an 850 m radius of the geophone are shown in Fig. 10. These slab avalanches ranged in size from a very small slab avalanche (avalanche 7; approximately 15 m wide and 50 m long) to the largest avalanche observed at our field site during the winter of 2010 (avalanche 2;

approximately 150 m wide and 350 m long). The seismic signals generated by these ten slab avalanches (Fig. 11) have signal amplitude and spectral characteristics very similar to those of loose snow avalanches (Fig. 7). The amplitude of the signals generated by slab avalanches mainly related to the distance between the avalanche and the sensor, and the majority of the energy was below 40 Hz. Again, the seismic signal of most slab avalanches had a characteristic spindle shape and higher frequencies were only associated with avalanches which released close to the sensor (avalanches 6 and 7 in Fig. 11).

Occasionally it was possible to identify signal characteristics only associated with slab avalanches. St.Lawrence and Williams (1976) and van Herwijnen and Schweizer (2011) observed first arrivals in the seismogram associated with weak layer fracture prior to slab avalanche release which distinguish slab avalanches from loose snow avalanches. While for avalanches that released close to the sensor such first arrivals were also observed, for other slab avalanches the seismic signal resembled that of a loose snow avalanche (Fig. 12). We were therefore not able to reliably identify the type of avalanche that released based on the generated seismic signal.

6. Avalanche activity

For the winter of 2010 we identified seismic signals generated by avalanches by visually comparing the seismogram with the spectro-gram, comparable to what is done in a system for the automatic detection of avalanches (Navarre et al., 2009). The date, time and duration of any signal which exhibited characteristics typical for avalanches were recorded. The duration of the signal was determined by visual inspection of the spectrogram. As can be seen in Figs. 7 and 11, the duration of avalanche generated signals as observed in the spectrogram was generally well defined. The onset was defined as the
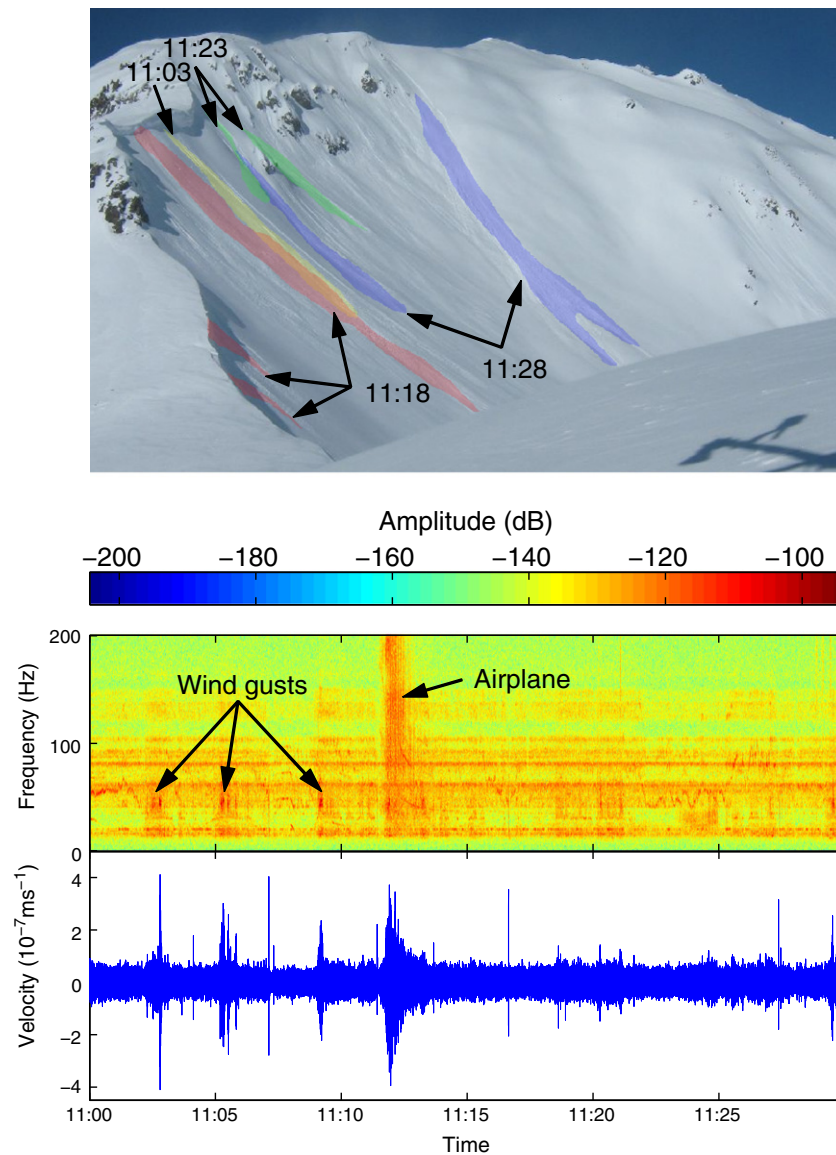
Fig. 8. Eight dry loose snow avalanches, observed on images from an automatic camera between 11:00 and 11:30 on 21 February 2010, that were not detected in the seismic data. The avalanches released at a distance between 200 and 350 m from the sensor. Top: contour of each avalanche and time the avalanche was first seen. Bottom: seismogram (bottom) and spectrogram (top) of 30 min of seismic data between 11:00 and 11:30. Signals with characteristics typical for avalanches were not detected.

first appearance of energetic low frequency signals (i.e. between 15 and 25 Hz), while the end of the signal was defined as the time when low frequency signals reverted back to background levels. Independent avalanche activity data were also derived from the automatic camera images. Avalanches were visually identified on the images and the time and date of the first image where the avalanche was seen was recorded.

In total, 385 seismic signals suspected to have been generated by avalanches were identified. Fewer avalanches were observed on the images of the automatic cameras (168). There were 34 days without any observed avalanches in the seismic data, while this number was much larger for the automatic cameras (82 days). This is not surprising since the geophone can detect avalanches in an area which is much larger than the field of view of the automatic cameras (Fig. 1) and poor visibility, for instance due to cloud cover or snowfall, essentially 'blinds' the cameras. Nevertheless, avalanche activity obtained from the seismic sensor and from the automatic cameras correlated well (Pearson $r = 0.54$; Fig. 13).

During the winter of 2010, avalanche activity increased markedly after 15 March 2010 (Fig. 13). In the avalanche activity data derived from the seismic sensor there were 17 days with increased avalanch-

ing (light blue bars in Fig. 13), defined as days with avalanche activity larger than the mean. The days with increased avalanche activity were all after 15 March 2010 and can be grouped into two longer avalanche cycles, from 19 to 24 March and from 19 to 30 April, and two short avalanche cycles around 29 March and 6 April. The periods of increased avalanche activity as derived from the images (orange squares in Fig. 13) coincided well with those from the seismic data with the exception of an avalanche cycle around 21 February. On 21 February loose snow avalanches seen on the images were not detected by the seismic sensor. These were primarily small dry loose snow avalanches caused by wind transport of recent new snow.

Information on the size and type of the avalanches detected in the seismic data was not available. However, the vast majority of avalanches observed on the images from the automatic cameras were loose snow avalanches (93%). It therefore stands to reason that the majority of avalanches detected in the seismic data were also loose snow avalanches. Furthermore, the majority of avalanches were most likely relatively small (i.e. short runout distance) since the generated seismic signals typically had a duration of less than 20 s (Fig. 14). Since avalanches are gravity driven, as a first approximation the runout
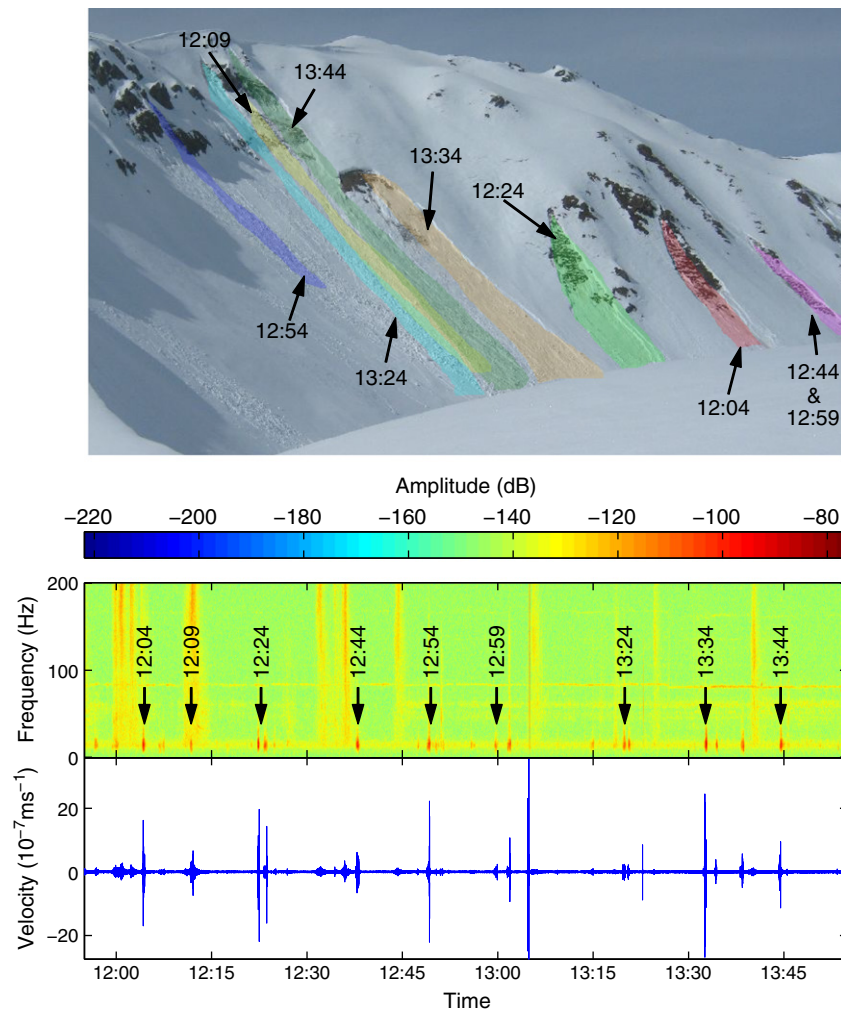
Fig. 9. Nine wet loose snow avalanches, observed on images from an automatic camera between 12:00 and 14:00 on 23 March 2010, that were detected in the seismic data. The avalanches released at a distance between 300 and 400 m from the sensor. Top: contour of each avalanche and time the avalanche was first seen. Bottom: seismogram (bottom) and spectrogram (top) of 2 h of seismic data between 12:00 and 14:00. Many signals with characteristics typical for avalanches were detected. Arrows in the spectrogram indicate signals likely generated by the avalanches observed in the images.

distance x of an avalanche can be expressed as $x \propto \frac{1}{2}at^2$, where a is the acceleration and t is the duration of the avalanche. The acceleration a is not constant and depends on several factors, such as slope, friction and the type of snow (e.g. Vilajosana et al., 2007a). However, if we assume a similar acceleration for all avalanches observed, the runout distance x directly relates to the square of the duration of the event. The cumulative distribution of t^2 obeyed a power law with an exponent of 2.5 ± 0.4 (inset Fig. 14), similar to the exponent of 2.2 ± 0.1 measured for snow slab avalanche scaling based on slab width (Faillettaz et al., 2004). Since for slab avalanches the size of the initial release relates to the runout distance (Bartelt et al., 1999), the agreement between the observed power law exponents suggests that the square of the duration of an event relates to the runout distance of the avalanche.

6.1. Comparison with meteorological data

Avalanche activity during the winter of 2010 was qualitatively compared with meteorological data from nearby AMSs. We focussed on the relation between avalanche activity derived from the seismic data with air temperature, changes in snow height (ΔHS) and mean wind speed. A quantitative statistical comparison between meteorological data and avalanche activity was not deemed meaningful since crucial information on avalanche type (e.g. type of weak layer, dry or wet snow) and location (e.g. aspect, elevation) was only scarcely

available. Furthermore, given the small investigation area, results from a detailed statistical analysis would only apply to avalanche release at our specific site.

It is well known that the influence of meteorological conditions on avalanching is complex. Common factors leading to avalanching are loading by precipitation or snow drift and warming (e.g. Schweizer et al., 2003). During the entire winter, avalanches were closely related to increases in snow height (Fig. 15b). Every snowfall was related to some avalanche activity either during the snowfall or up to two days after the snowfall. Furthermore, days with high mean wind speed frequently coincided with avalanching (Fig. 15c). Finally, during the second half of the winter, high mean daily air temperature was related to increases in avalanche activity (Fig. 15a).

Above average avalanche activity was most closely related to changes in snow height and mean air temperature (Fig. 15). Periods of increased avalanche activity always occurred within four days of snowfall (Fig. 15b) and the mean air temperature was typically close to or above freezing (Fig. 15a). Based on the meteorological data it is clear that two different processes were related to periods of increased avalanche activity. Around 23 March and at the end of April the mean daily air temperature was consistently above 0 °C (Fig. 15a) and the snow height steadily decreased (Fig. 15b). Since the snow was likely cohesionless and isothermal, avalanches were therefore able to entrain a large portion of the snow cover. On the other hand, on 29
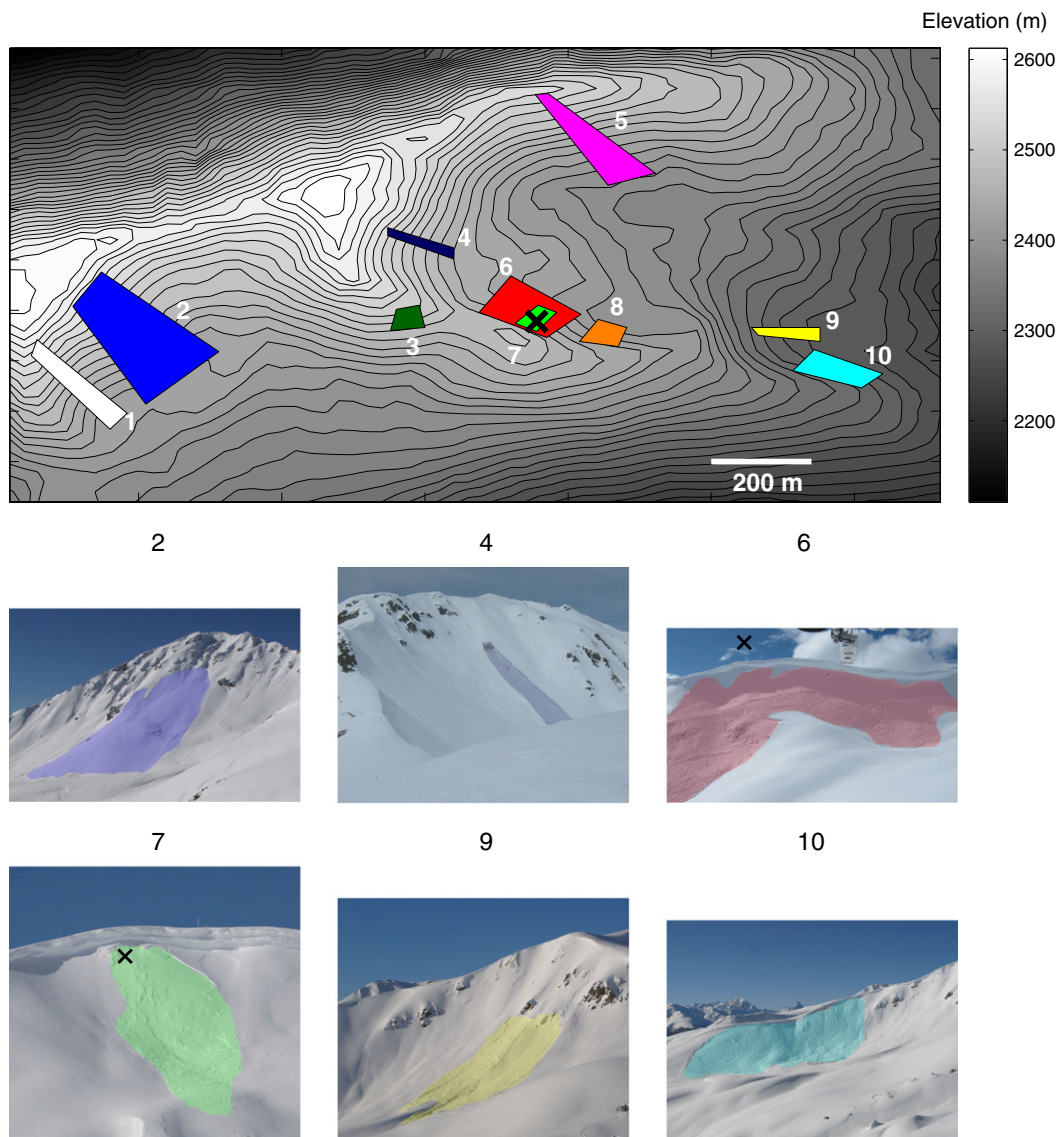
Fig. 10. Location of ten slab avalanches, observed on the images from automatic cameras or by field workers, that were detected in the seismic data. Top: approximate location and runout distance for each avalanche. The location of the geophone is marked with a black cross. Bottom: images from automatic cameras and photographs with the contour for six avalanches. For avalanche 6 and 7 the location of the geophone is marked with a black cross.

March and 9 April the mean air temperature was only briefly close to zero degrees, therefore only the recent new snow was unstable.

7. Discussion and conclusions

Continuous seismic data from a geophone inserted in the snow cover in an avalanche start zone were analyzed with a particular view on seismic signals generated by avalanches. Based on field observations and images from automatic cameras we were able to detect numerous seismic signals generated by avalanches. By visually analyzing the spectrogram of the seismic data, signals generated by avalanches were distinguished from environmental noise, confirming results presented by Biescas et al. (2003) and Navarre et al. (2009). This enabled us to qualitatively confirm general characteristics of seismic signals generated by avalanches and to derive avalanche activity data for the winter of 2010. In combination with avalanche activity data obtained from automatic cameras and meteorological data from nearby automatic meteorological stations, this constitutes a unique record of basin scale avalanche activity for an entire winter season.

Over 380 seismic signals generated by avalanches were identified by visual inspection of the data. Since the exact number of avalanches that released is unknown, we cannot determine the success rate of avalanche detection. However, our field observations suggest that slab avalanches are better detected than loose snow avalanches. Every slab avalanche that was observed on the images from the automatic cameras or during field observations was detected in the seismic data. On the other hand, numerous loose snow avalanches were observed but not detected by the seismic sensor (Fig. 8). This is perhaps due to the fact that the mass of snow involved in slab avalanches is generally larger.

The majority of studies relating seismic signals to snow avalanches used geophones embedded in an avalanche track or at valley bottom (e.g. Biescas et al., 2003; Nishimura and Izumi, 1997; Suriñach et al., 2001). Given the large distance between the seismic sensor and the avalanche start zone, only relatively large avalanches were detected and studied. For the SLF test site in Western Switzerland and using different sensors, Biescas et al. (2003) determined that avalanches with a runout distance of less than 600 m which stopped more than 2 km away from the sensor could not be detected. By inserting the seismic sensor directly in an avalanche start zone we were able to
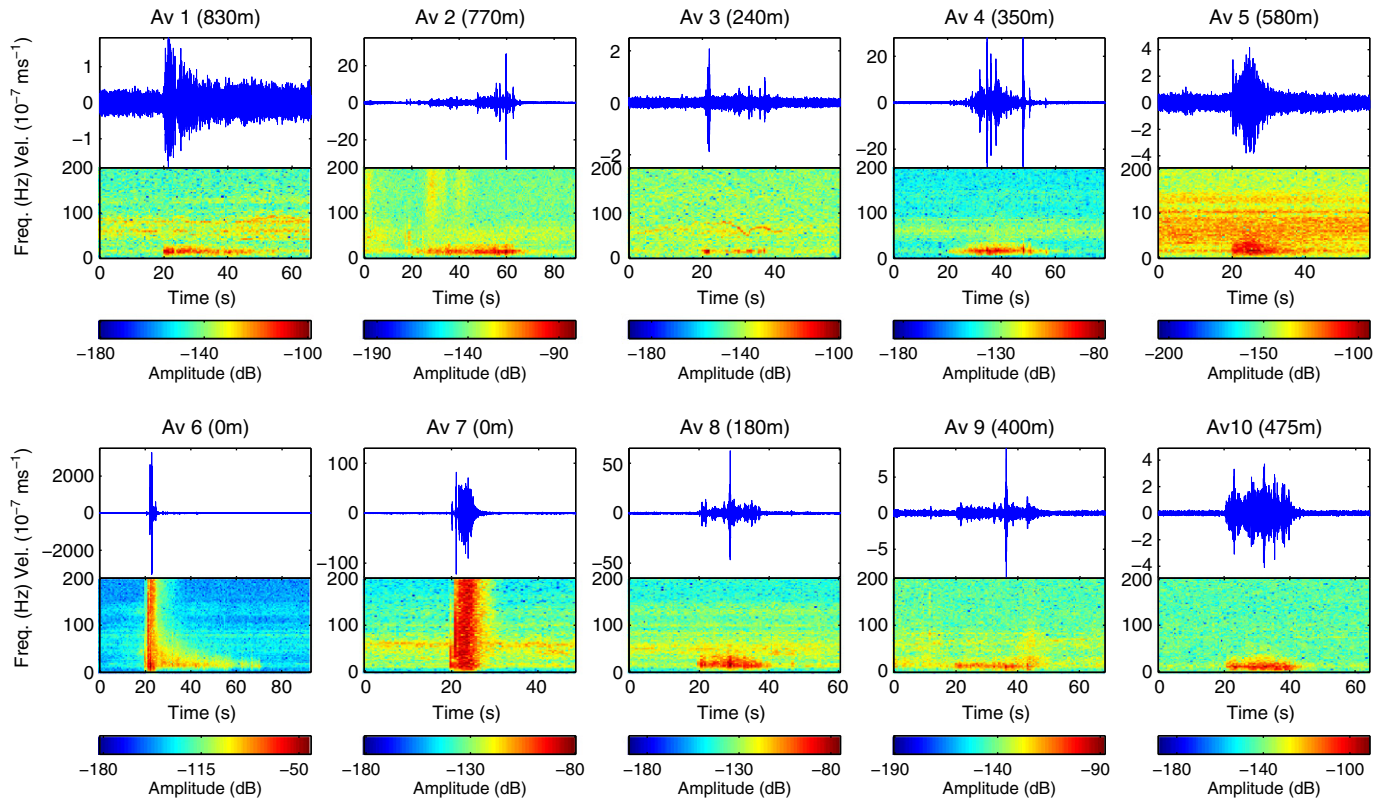
Fig. 11. Seismic signals generated by the ten slab avalanches shown in Fig. 10. For each avalanche the seismogram (top) and spectrogram (bottom) are shown. The approximate distance to the geophone is also given (in brackets).

detect many small avalanches, including loose snow avalanches. The avalanches we observed were much smaller than the size of avalanches discussed in previous studies (e.g. Biescas et al., 2003; Nishimura and Izumi, 1997; Suriñach et al., 2001). This comes as no

surprise, since signals that originate closer to the sensor are better detected.

The observed patterns in the signals generated by different types of avalanches confirmed previous work based on seismic signals generated by larger avalanches. We typically observed a spindle shaped signal, increases in signal amplitude were attributed to the impact of the flowing snow mass with terrain features and we observed a time frequency content and signal amplitude which mainly depended on the distance between the avalanche and the sensor (Figs. 7 and 11), confirming earlier findings (e.g. Biescas et al., 2003; Nishimura and Izumi, 1997; Suriñach et al., 2001). Our results also confirmed that wet
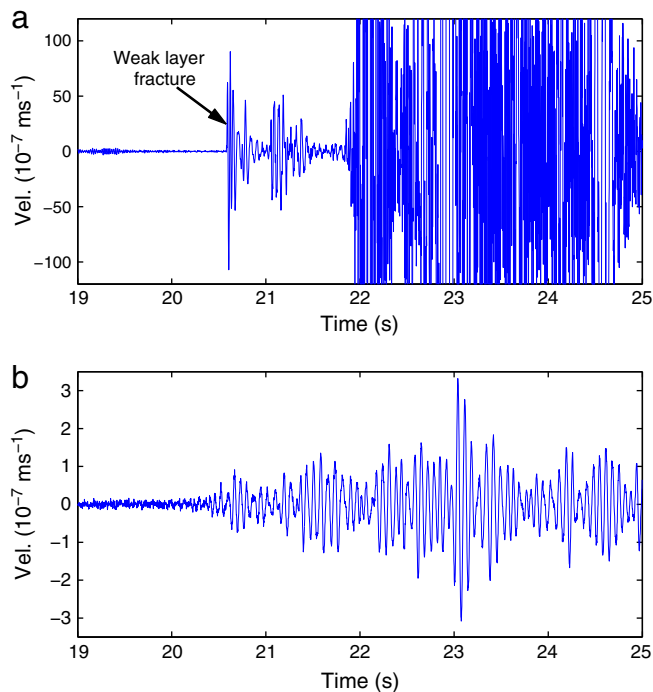

Fig. 12. First 6 s of the seismic signals generated by slab avalanche 6 (a) and 10 (b) shown in Fig. 11. First arrivals associated with weak layer fracture were observed for avalanche 6 but not for avalanche 10.
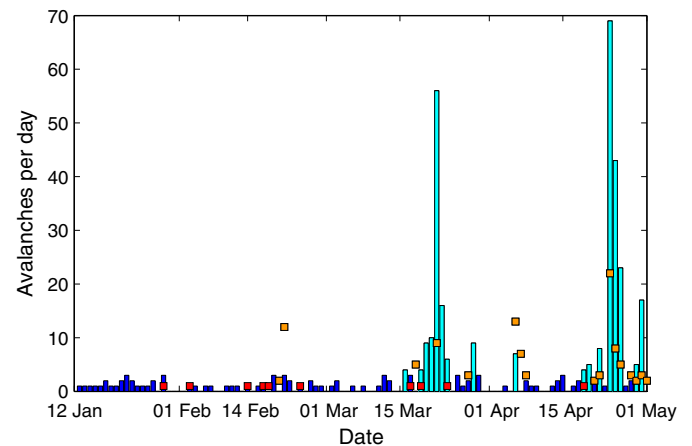

Fig. 13. Comparison between avalanche activity data obtained from the seismic sensor (blue bars) and from the automatic cameras (red squares). Days with increased avalanche activity, defined as days with avalanche activity larger than the mean, are highlighted with light blue bars for the seismic data and orange squares for the camera data. More avalanches were detected with the seismic sensor than on the images from the automatic cameras.
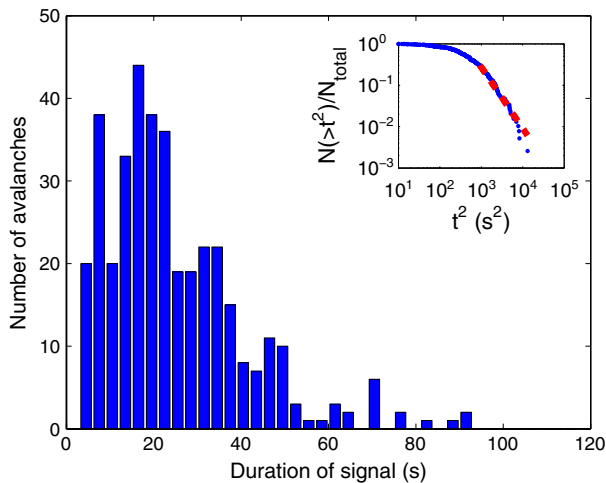
Fig. 14. Distribution of the duration of seismic signals generated by avalanches. Inset: Cumulative distribution of the square of the duration (t^2). The power law Exponent value is 2.5 ± 0.4, as estimated by the maximum likelihood method for signals longer than 30 s (dashed line).

snow avalanches generate larger seismic signals then dry snow avalanches of comparable size, as reported by Biescas et al. (2003). St.Lawrence and Williams (1976) and van Herwijnen and Schweizer (2011) suggested that first arrivals in the seismogram associated with weak layer fracture prior to slab avalanche release can distinguish slab avalanches from loose snow avalanches. While in some cases we observed such first arrivals (Fig. 12), with the equipment we used at our field site we were not able to reliably identify the type of avalanche that released based on the generated seismic signal.

Avalanche activity obtained from the seismic sensor and from the automatic cameras were in good agreement (Fig. 13). This strengthens our confidence that the signals identified in the seismic data were generated by avalanches. It also shows that automatic cameras can be useful tools to observe avalanching, including small dry loose snow avalanches, which were typically not detected in the seismic data. However, our results also show that due to limited visibility and a limited field of view, avalanche activity determined using automatic cameras is underestimated and that the timing can be imprecise (Fig. 13). On the other hand, with the seismic sensor at our field site we were able to reliably determine the time of release of avalanches over an area of about 2 km².

Comparison of avalanche activity data in combination with meteorological data confirmed commonly followed rules in avalanche forecasting. Each snowfall and increases in wind speed resulted in avalanche activity (Fig. 15). On the other hand, several days of positive mean daily air temperature and snow settlement were associated with two large wet snow avalanche cycles. These observations are consistent with results from a study on wet snow avalanche formation (Baggi and Schweizer, 2009). Even though we only presented data from one winter, our results suggest that while avalanche detection using seismic methods can provide reliable and accurate avalanche activity data for avalanche forecasting, combined with meteorological data it can also provide insight into avalanche formation processes.
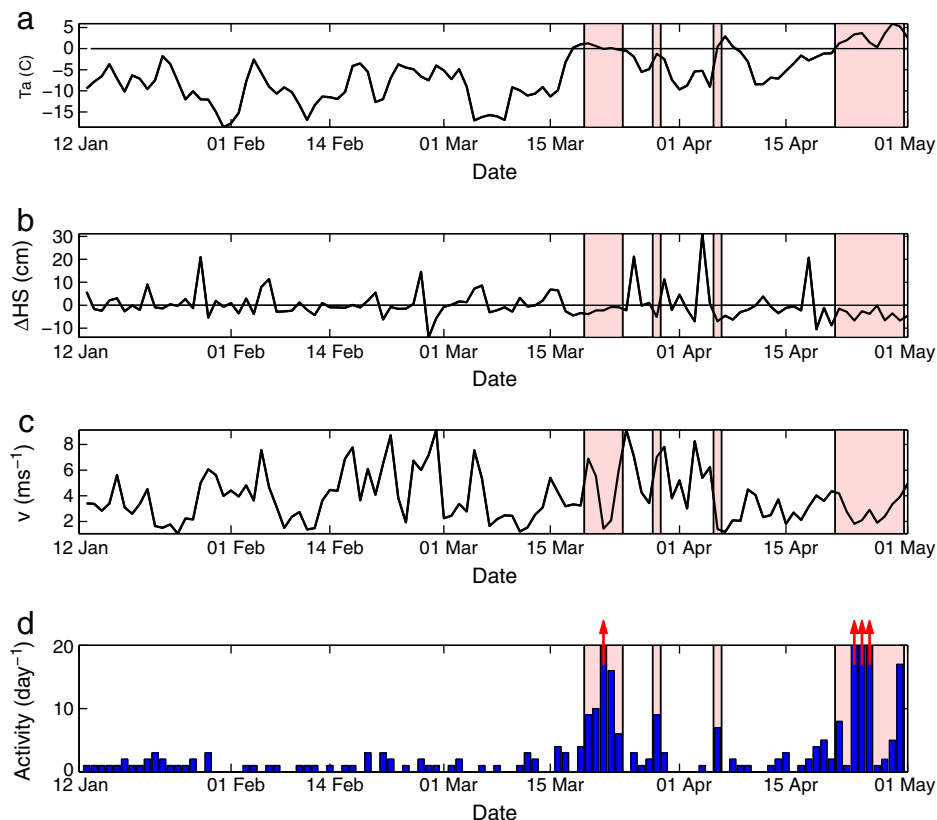
Acknowledgements

Fig. 15. Comparison between meteorological data and avalanche activity obtained from the seismic data. (a) Mean daily air temperature (Ta). (b) Mean daily change in snow height (ΔHS). (c) Mean daily wind speed (v). (d) Avalanche activity. Four periods with increased avalanche activity are highlighted (shaded areas).

References

Baggi, S., Schweizer, J., 2009. Characteristics of wet-snow avalanche activity: 20 years of observations from a high alpine valley (Dischma, Switzerland). Nat. Hazards 50 (1), 97–108.

Bartelt, P., Salm, B., Gruber, U., 1999. Calculating dense-snow avalanche runout using a Voellmy fluid model with active/passive longitudinal straining. J. Glaciol. 45 (150), 242–254.

Bessason, B., Eiriksson, G., Thorarinsson, O., Thorarinsson, A., Einarsson, S., 2007. Automatic detection of avalanches and debris flows by seismic methods. J. Glaciol. 53, 461–472.

Biescas, B., Dufour, F., Furdada, G., Khazaradze, G., Suriñach, E., 2003. Frequency content evolution of snow avalanche seismic signals. Surv. Geophys. 24, 447–464.

Buckingham, M., Giddens, E., Simonet, F., Hahn, T., 2002. Propeller noise from a light aircraft for low-frequency measurements of the speed of sound in a marine sediment. J. Comput. Acoust. 10, 445–464.

Deparis, J., Jongmans, D., Cotton, F., Baillet, L., Thouvenot, F., Hantz, D., 2008. Analysis of rock-fall and rock-fall avalanche seismograms in the French Alps. Bull. Seismol. Soc. Am. 98, 1781–1796.

Faillettaz, J., Louchet, F., Grasso, J.R., 2004. Two-threshold model for scaling laws of noninteracting snow avalanches. Phys. Rev. Lett. 93, 208001.

Lay, T., Wallace, T., 1995. Modern global seismology. Academic Press, San Diego, California.

Leprettre, B., Navarre, J., Panel, J., Touvier, F., Taillefer, A., Roulle, E., 1998. Prototype for operational seismic detection of natural avalanches. Ann. Glaciol. 26, 313–318.

McClung, D.M., Schaerer, P., 2006. The Avalanche Handbook. The Mountaineers, Seattle, Washington, U.S.A.

Navarre, J., Bourtova, E., Roulle, J., Deliot, Y., 2009. The seismic detection of avalanches: an information tool for the avalanche forecaster. In: Schweizer, J., van Herwijnen, A. (Eds.), International Snow Science Workshop ISSW, Davos, Switzerland, 27 September–2 October 2009. Swiss Federal Institute for Forest Snow and Landscape Research WSL, pp. 379–383.

Nishimura, K., Izumi, K., 1997. Seismic signals induced by snow avalanche flow. Nat. Hazards 15, 89–100.

Sabot, F., Naaim, M., Granada, F., Suriñach, E., Planet, P., Furada, G., 1998. Study of avalanche dynamics by seismic methods, image-processing techniques and numerical models. Ann. Glaciol. 26, 319–323.

Schweizer, J., Jamieson, J., Schneebeli, M., 2003. Snow avalanche formation. Rev. Geophys. 41, 1016.

Scott, E., Hayward, C., Kubichek, R., Hamann, J., Pierre, J., Comey, B., Mendenhall, T., 2007. Single and multiple sensor identification of avalanche-generated infrasound. Cold Reg. Sci. Technol. 47 (1–2), 159–170.

St.Lawrence, W., Williams, T., 1976. Seismic signals associated with avalanches. J. Glaciol. 17, 521–526.

Suriñach, E., Sabot, F., Furdada, G., Vilaplana, J., 2000. Study of seismic signals of artificially released snow avalanches for monitoring purposes. Phys. Chem. Earth Pt. B 25, 721–727.

Suriñach, E., Furdada, G., Sabot, F., Biescas, B., Vilaplana, J., 2001. On the characterization of seismic signals generated by snow avalanches for monitoring purposes. Ann. Glaciol. 32 (7), 268–274.

Suriñach, E., Vilajosana, I., Khazaradze, G., Biescas, B., Furdada, G., Vilaplana, J., 2005. Seismic detection and characterization of landslides and other mass movements. Nat. Hazards Earth Syst. Sci. 5 (6), 791–798.

van Herwijnen, A., Schweizer, J., 2011. Seismic sensor array for monitoring an avalanche start zone: design, deployment and preliminary results. J. Glaciol. 57, 257–264.

Vilajosana, I., Khazaradze, G., Suriñach, E., Lied, E., Kristensen, K., 2007a. Snow avalanche speed determination using seismic methods. Cold Reg. Sci. Technol. 49, 2–10.

Vilajosana, I., Suriñach, E., Khazaradze, G., Gauer, P., 2007b. Snow avalanche energy estimation from seismic signal analysis. Cold Reg. Sci. Technol. 50, 72–85.